Massively Parallel Hybrid TLM-PEEC Solver and Model Order Reduction for 3D Nonlinear Electromagnetic Transient Analysis

Madhawa Ranasinghe, *Student Member, IEEE*, and Venkata Dinavahi, *Fellow, IEEE*

***Abstract*—Electromagnetic (EM) equipments are ubiquitous in electrical power generation, transmission, and distribution systems, and they should be studied for reliable and continuous operation under switching operations, faults, and other transient conditions. Conventional lumped models lack the capability to consider EM field interactions, while distributed methods, such as the finite element method (FEM), are widely employed to address these interactions. The partial element equivalent circuit (PEEC) method has gained interest in EM modeling due to its equivalent circuit behavior and its potential for optimization using circuit solver techniques. This article extends the hybrid transmission line modeling (TLM)-based PEEC 2-D solver for 3-D EM transient simulations, providing detailed information on the matrix solver, time-domain algorithm, the parallelized the Newton–Raphson (N–R) solver for nonlinear magnetics, and a suitable model order reduction (MOR) method. The hybrid TLM–PEEC technique decouples the nonlinear elements from the linear network, providing individual solutions for each unknown through N–R iterations, thereby enabling parallel computing. The proper orthogonal decomposition method, a MOR technique, was integrated into the hybrid TLM–PEEC method to improve performance by removing unnecessary features in the system. The parallelization of the methods has been fully explored and implemented on both many-core graphics processing unit and multicore central processing unit, enabling field-oriented transient simulation for a 3-phase 3-D core-type transformer coupled with external circuits, as well as quasi-static 3-D simulation for a high-voltage insulator. The accuracy and computational efficiency of the proposed architectures were verified through simulation results obtained from similar case studies implemented in Comsol Multiphysics.**

***Index Terms*—3-D modeling, circuit modeling, computational electromagnetics (EMs), electromagnetic transients (EMTs), graphics processing unit (GPU), integral equations, nonlinear systems, parallel processing, partial element equivalent circuit (PEEC) method, proper orthogonal decomposition (POD) method, time-domain solver, transmission line modeling (TLM) method.**

I. Introduction

Electromagnetic (EM) simulation is a crucial step in the field of engineering for modeling and analyzing EM fields, along with their interactions with external devices and materials. It is an efficient way of understanding behavior and optimizing systems without costly, time-consuming physical experiments. Electromagnetic transient simulation (EMT) involves analyzing the EM behavior of systems over time in response to sudden changes or disturbances. Power system EM equipment is a critical component of electric power transmission, distribution, and operating systems and should remain operational under both normal and abnormal grid conditions and equipment faults for economic efficiency [1]. Therefore, it is essential to understand the behavior of the EM equipment during faults, switching operations, and other transient conditions.

Conventional lumped circuit models [2], [3] are popular in power system equipment modeling. Lumped models for electromagnetic passive systems and power system lightning surge analysis are presented [4], [5], but they exhibit drawbacks when visualizing EM fields across the systems. Incorporating field-oriented Maxwell's equations is crucial for solving material properties and understanding the system's physics in such scenarios. Often, obtaining analytical solutions for Maxwell's equations in power system applications is impossible due to their complexity and nonlinearity. Numerical methods are utilized to solve EMT problems devoid of analytical solutions, and the following are the commonly employed methods in power system applications [6]. Differential techniques, such as the finite difference time domain (FDTD) methods, the finite element method (FEM) and the transmission line modeling (TLM) method are applied in the modeling of power systems, with FEM playing a major role due to its ability to handle complex geometries and ensure higher accuracy. Integral methods such as the method of moments (MoMs) and the partial element equivalent circuit (PEEC) method have gained prominence in solving EM problems due to their ability to solve the domain effectively by addressing only the discretization of magnetizable regions. Therefore, due to the exclusion of air regions and the avoidance of unnecessarily larger computational domains over the problem, integral methods require fewer spatial elements compared to differential methods for a particular EM problem.

Among integral techniques, the PEEC method has gained significant interest due to its equivalent circuit behavior, providing flexibility in solutions and the potential for optimization using circuit solver techniques. This method is fascinating as it facilitates the transformation of the specific EM problem into the circuit domain by establishing PEEC equivalent circuits

Received 24 April 2024; revised 23 August 2024; accepted 14 September 2024. This work was supported by the Natural Sciences and Engineering Research Council of Canada (NSERC). *(Corresponding author: Madhawa Ranasinghe.)*

The authors are with the Department of Electrical and Computer Engineering, University of Alberta, Edmonton, AB T6G 1H9, Canada (e-mail: donlucks@ualberta.ca; dinavahi@ualberta.ca).

Color versions of one or more figures in this article are available at https://doi.org/10.1109/TEMC.2024.3462928.
Digital Object Identifier 10.1109/TEMC.2024.3462928

for each element within the spatial domain. The inductive [7] and capacitive [8] effects of conductors are considered key components in this approach, initially introduced for the EM modeling of multiconductor systems [9] and later extended to include dielectric materials [10]. The modeling of linear magnetic materials [11] paved the way for a broad spectrum of applications using the PEEC method, and its utilization was expanded through the development of mathematical models for the solver [12], [13], [14], [15]. Subsequently, these models were further extended to include nonlinear magnetic materials [16], while formulating comprehensive analytical formulas for the coupling of electric and magnetic fields [17].

The PEEC method is applicable to both static and dynamic EM scenarios. In steady-state applications where voltages and currents remain stable over time, a dc PEEC solution is suggested and has been utilized for interconnect analysis [18]. An electrostatic solution is proposed using piecewise basis functions and has been applied to applications based on curved 3-D geometry [19], comparing its accuracy with the FEM method. The majority of PEEC applications rely on quasi-static assumptions [20], [21], functioning effectively for low-frequency applications and versatile for implementation in power system applications.

The PEEC solution can be expressed in either the time domain or frequency domain [22], with the time-domain approach being particularly beneficial for analyzing EMTs in power system apparatus. A hybrid PEEC-SPICE solver has been introduced for addressing nonlinear EM problems, achieving the optimal circuit solution through circuit simulations performed in OrCAD [23]. A nonlinear adaptive time-domain solver [16] for the PEEC method has been implemented and applied to a closed magnetic circuit for accuracy comparison in field calculations against FEM. The transient analysis of transmission tower lightning surges was performed using a hybrid FDTD-PEEC technique [24], where the FDTD method was employed for conducting time-domain calculations. Hybrid approaches efficiently enhance the performance of the PEEC solver by integrating parallelism and optimizing the circuit solution.

The TLM method, initially developed for analyzing wave propagation [25], has been expanded to nonlinear lumped circuit analysis due to its ability to handle circuit networks using TLMs [26]. The method has been further extended to numerically simulate power circuits, emphasizing the elimination of repetitive solvers for nonlinearities, thus improving runtime while maintaining stability [27]. The TLM method enables the decoupling of multiple nonlinear elements from the linear network, allowing independent resolution of these nonlinearities using dedicated solvers like the Newton–Raphson (N–R) method [28]. This approach has been coupled with FEM and is ideal for solving nonlinear EM problems, leading to computational efficiency [29]. The TLM method has proven feasible for integration with the PEEC method, and the hybrid TLM-PEEC 2D approach has demonstrated greater computational efficiency through parallel computing while maintaining high accuracy compared to FEM [30].

Model order reduction (MOR) techniques offer a way to reduce system complexity by removing unnecessary features while retaining the required accuracy. The proper orthogonal decomposition (POD) method originally developed in 1967 [31], was applied to reduce the high dimensionality of large FEM simulations [32], [33], [34]. It has been successfully used to perform real-time power system transient simulations [35]. The PEEC method often involves larger dimensions, and therefore the POD method has been integrated into the proposed hybrid TLM-PEEC method to reduce the size of simulated systems.

This article aims to introduce the hybrid TLM-PEEC method for 3-D EM equipment transient simulation, focusing on the decoupling of the N–R solver for nonlinear magnetic materials. The proposed method will be applied to investigate EMTs in a 3-phase 3-D core-type transformer by incorporating coil structures modeled with distributed conductor elements, offering a detailed representation of both primary and secondary windings across all phases. The POD method has been applied to the hybrid TLM-PEEC architecture, demonstrating significant performance improvements. In addition, the method will be extended to solve 3-D electrostatic applications, demonstrating the versatility of this approach in studying EM fields within transmission line high-voltage insulators. The parallelism of the methods is fully explored [36] by implementing it through the compute unified device architecture (CUDA) application programming interface (API), enabling simulations to be conducted on the Nvidia Tesla V100 graphics processing unit (GPU) within a parallel architecture. The transient results obtained from the hybrid TLM–PEEC method are compared with those obtained from similar case studies performed using the commercial FEM software Comsol Multiphysics for accuracy and computational efficiency.

The rest of this article is organized as follows. Section II provides the standard PEEC formulation for conductors, including nonlinear magnetic materials, and presents the matrix system formulation to obtain the solution. Section III describes the hybrid TLM-PEEC solution for 3-D systems and its matrix system formulation by decoupling the nonlinear elements from the linear network; including the algorithms to achieve the time-domain EMT simulation. Section IV provides the implementation of the POD method and its integration with the hybrid TLM-PEEC architecture, proposing the POD-TLM-PEEC approach. In Section V, the design of the hybrid TLM-PEEC 3-phase 3-D core-type transformer model and high-voltage insulator model is presented, along with their simulation results. Finally, Section VI concludes this article.

II. Standard PEEC Formulation

The basic PEEC formulation relies on the volumetric equivalent principle of Maxwell's equations. It starts with the electric field integral equation (EFIE) and continuity equation, providing a set of integral equations that can be solved numerically. Partial elements are defined for each of the integral equations, offering a circuit interpretation that can be addressed using circuit solver methods. The PEEC method is initiated by discretizing magnetizable materials, conductors, dielectrics, and magnetic materials. In this formulation, both conductors and magnetic materials are taken into consideration, and the materials are

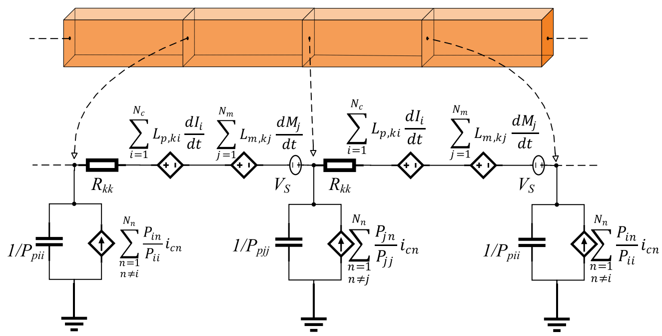

Fig. 1. PEEC equivalent circuit for a 3-D conductor wire.

discretized into small-volume cells and surface cells. Electrical current, magnetic current, and charge densities are expanded using basis functions according to the discretization pattern, providing unknown densities in each cell to be solved. Rectangular basis functions are popular, as the unknown current densities and charge densities can be represented as constants over the volume and surface cells.

The Galerkin weighting process is employed on the discretized EFIE using an orthogonal set of basis functions to formulate a system of equations for solving unknown densities. As illustrated in Fig. 1, this formulation leads to the electrical circuit representation of the discretized EFIE, defining partial resistance, partial inductance, and coefficients of potentials as circuit elements. The coupling between electric and magnetic fields is also considered, and it is incorporated by adding an equivalent voltage source due to time-varying magnetization. By enforcing Kirchhoff's Voltage Law (KVL), Kirchhoff's Current Law (KCL), and the constitutive relation for nonlinear magnetic materials on the PEEC equivalent circuit, the following matrix representation can be obtained:

$$-\mathbf{A}\Phi(t) = \mathbf{V}_s(t) + \mathbf{R}\mathbf{I}(t) + \mathbf{L}_p\frac{d\mathbf{I}(t)}{dt} + \mathbf{L}_m\frac{d\mathbf{M}(t)}{dt} \tag{1}$$

$$\mathbf{P}^{-1}\frac{d\Phi(t)}{dt} - \mathbf{A}^T\mathbf{I}(t) = \mathbf{I}_s(t) \tag{2}$$

$$\mathbf{D}\mathbf{I}(t) + \mathbf{T}(|\mathbf{H}(t)|)\mathbf{M}(t) = -\mathbf{G}\mathbf{I}_s(t) \tag{3}$$

where

$\mathbf{R}$	Partial resistance matrix.
$\mathbf{L}_p$	Partial inductance matrix.
$\mathbf{P}$	Partial coefficient of potential matrix.
$\mathbf{L}_m$	Matrix representing induced effects from magnetic fields.
$\mathbf{A}$	Incidence matrix.
$\mathbf{D}$	Matrix representing magnetic fields due to electrical currents.
$\mathbf{T}$	Matrix representing magnetic fields due to magnetization.
$\mathbf{G}$	Matrix representing magnetic fields due to source currents.
$\mathbf{V}_s$	Voltage source vector due to external fields.
$\mathbf{I}_s$	Lumped current source vector.
$\Phi(t)$	Nodal voltage vector.
$\mathbf{I}(t)$	Branch current vector.
$\mathbf{M}(t)$	Magnetization vector.

The matrix $\mathbf{T}$ can be separated into two components, representing a linear matrix $\mathbf{W}$ and a nonlinear diagonal matrix $\Omega(|\mathbf{H}(t)|)$, as given follows [16]:

$$\mathbf{T}(|\mathbf{H}(t)|) = \mathbf{W} + \Omega(|\mathbf{H}(t)|). \tag{4}$$

The nonlinear elements in the diagonal matrix depend on the relative permeability $\mu_r(|\mathbf{H}(t)|)$ of the material, which, in turn, relies on the magnetic field $\mathbf{H}(t)$ of the corresponding nonlinear element and can be expressed as follows:

$$\Omega(|\mathbf{H}(t)|) = -\frac{\mu_0\mu_r(|\mathbf{H}(t)|)}{\mu_r(|\mathbf{H}(t)|) - 1}. \tag{5}$$

Equations (1)–(5) describe the set of equations to formulate a matrix system for obtaining the solution vector, expressed as follows:

$$\begin{bmatrix} \mathbf{A} & \mathbf{R}+\mathbf{L}_p\frac{d}{dt} & \mathbf{L}_m\frac{d}{dt} \\ \mathbf{P}^{-1}\frac{d}{dt} & -\mathbf{A}_T & \mathbf{0} \\ \mathbf{0} & \mathbf{D} & \mathbf{T}(|\mathbf{H}(t)|) \end{bmatrix} \begin{bmatrix} \Phi(t) \\ \mathbf{I}(t) \\ \mathbf{M}(t) \end{bmatrix} = \begin{bmatrix} -\mathbf{V}_s \\ \mathbf{I}_s \\ -\mathbf{G}\mathbf{I}_s \end{bmatrix}. \tag{6}$$

The PEEC solution consists of vectors $\Phi(t)$, $\mathbf{I}(t)$, and $\mathbf{M}(t)$ with sizes N_n, N_l, and $3N_m$, representing the number of nodes, number of branches, and three times the number of magnetic elements in the PEEC network, respectively. The matrix $\mathbf{A}$ is filled based on the current direction between two adjacent nodes, and +1 or -1 is assigned following the modified nodal analysis (MNA) theory. Partial resistance calculations for $\mathbf{R}$ and partial self-inductance calculations to fill diagonal elements of the matrix $\mathbf{L}_p$ are presented in [37]. Meanwhile, analytical formulas to fill off-diagonal terms representing partial mutual inductance calculations are processed in [38]. Partial coefficients of potentials are detailed in [39], presenting analytical formulas for different geometries. Analytical formulas to fill matrices $\mathbf{D}$, $\mathbf{G}$, $\mathbf{L}_m$, and $\mathbf{W}$ are available in [12] and [17]. For nonlinear magnetic materials, where the relationship between magnetic flux density and magnetic field intensity is not linear, the calculation of matrix $\mathbf{T}(|\mathbf{H}(t)|)$ is not trivial, and it should follow an iterative numerical approach, such as the N–R method [16], to approximate the solution. The solver described in (6) represents the standard PEEC solver, and with accurate partial element calculations, it can be applied to any 3-D EM applications.

III. Proposed Hybrid TLM–PEEC Formulation

The standard PEEC nonlinear solver can be parallelized using the TLM method while using discrete models for linear and nonlinear elements in the PEEC equivalent circuit. This allows for the decoupling of the nonlinear elements from the linear network, enabling the independent solution of the nonlinear elements using individual N–R iterations. The PEEC nonlinear system can be expressed as the PEEC equivalent circuit with linear elements, as shown in Fig. 2(a) and a magnetic current-based nonlinear circuit, as depicted in Fig. 2(d) representing the constitutive relation of the nonlinear magnetic material [30].

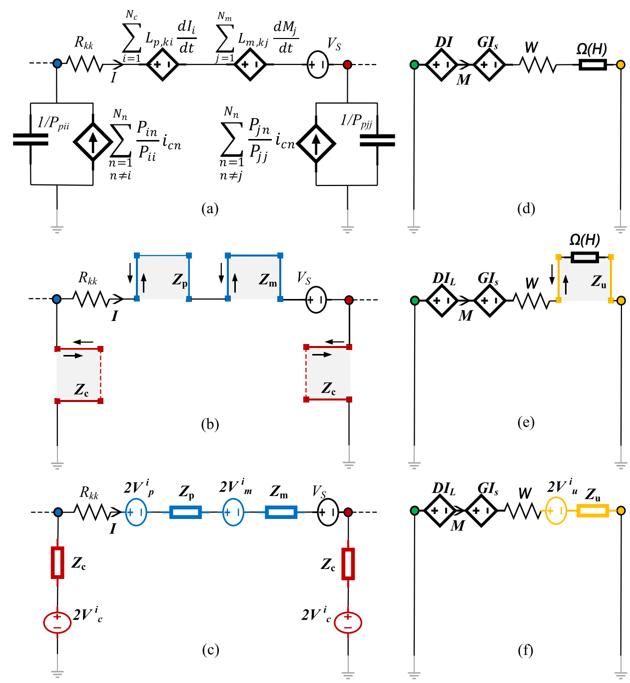

Fig. 2. Hybrid TLM–PEEC equivalent circuit model. (a) Linear network. (b) TLM model: scattering. (c) TLM model: gathering. (d) Nonlinear network. (e) TLM model: scattering. (f) TLM model: gathering.

The nonlinear diagonal matrix $\Omega(|\mathbf{H}(t)|)$, with a size of $3N_m$ corresponding to the 3-D Cartesian components aims to isolate the nonlinear components as $3N_m$ resistors. After enforcing TLM theory, these nonlinear resistors can be solved individually in parallel using N–R iterations.

According to the transmission line theory, a linear inductor can be represented as a lossless transmission line short-circuited at the far end with characteristic impedance $Z_L = 2L/\Delta t$, where L and Δt are inductance and round trip of the traveling waves on the line, respectively. A linear capacitor can be modeled as a lossless transmission line open-circuited at the far end with the characteristic impedance $Z_C = \Delta t/2C$. The voltage across the inductor and the capacitor can be expressed as the sum of the incident voltage and reflected voltage from each transmission line. The incident voltage pulse for the next time step can be expressed using the reflected voltage pulse and the reflection coefficient of each line, which is -1 for a short-circuited line and +1 for an open-circuited line. This process can be continued iteratively over the simulation period to obtain the transient results. A nonlinear resistor can be represented using a lossless transmission line with arbitrary characteristic impedance Z_u. Similar to linear elements, the voltage across the nonlinear element can be expressed as the sum of the incident voltage and the reflected voltage. The nonlinear voltage and current relationship of the resistor can be substituted using incident and reflected voltage pulses to obtain a decoupled nonlinear equation, which can be solved independently through N–R iterations to determine the incident voltage pulse for the next time step.

KVL can be enforced on the capacitive and inductive branches of the hybrid TLM–PEEC equivalent circuit, as illustrated in Fig. 2(c), and on the nonlinear magnetic circuit shown in Fig. 2(f), to obtain the hybrid TLM–PEEC equivalent circuit equations, which can be expressed as [30] follows:

$$-\mathbf{A}\Phi(t) = \mathbf{V}_s(t) + \mathbf{R}\mathbf{I}(t) + \mathbf{Z}_p\mathbf{I}(t) + 2\mathbf{V}_p^i[\mathbf{1}]_{N_l} + \mathbf{Z}_m\mathbf{M}(t) + 2\mathbf{V}_m^i[\mathbf{1}]_{3N_m} \quad (7)$$

$$\Phi(t) = \mathbf{Z}_c\mathbf{A}^T\mathbf{I}(t) + \mathbf{Z}_c\mathbf{I}_s(t) + 2\mathbf{V}_c^i[\mathbf{1}]_{N_n} \quad (8)$$

$$\mathbf{D}\mathbf{I}(t) + (\mathbf{W} + \mathbf{Z}_u)\mathbf{M}(t) = -\mathbf{G}\mathbf{I}_s(t) - 2\mathbf{V}_u^i \quad (9)$$

where

$\mathbf{Z}_p$	Surge impedance form $\mathbf{L}_p$ matrix.
$\mathbf{Z}_c$	Surge impedance form $\mathbf{P}$ matrix.
$\mathbf{Z}_m$	Surge impedance form $\mathbf{L}_m$ matrix.
$\mathbf{Z}_{u,vect}$	Arbitrary surge impedance vector.
$\mathbf{Z}_u$	Diagonal matrix from $\mathbf{Z}_{u,\text{vect}}$.
$\mathbf{V}_p^i$	Incident voltage matrix for $\mathbf{Z}_p$.
$\mathbf{V}_m^i$	Incident voltage matrix for $\mathbf{Z}_m$.
$\mathbf{V}_c^i$	Incident voltage matrix for $\mathbf{Z}_c$.
$\mathbf{V}_u^i$	Incident voltage vector for $\mathbf{Z}_{u,\text{vect}}$.
$[\mathbf{1}]_x$	Vector with size x and elements equal to 1.

Equations (7)–(9) describe the fundamental equations to formulate a matrix system for the hybrid TLM–PEEC method, and it can be expressed as follows:

$$\begin{bmatrix} \mathbf{R}+\mathbf{Z_p}+\mathbf{A}\mathbf{Z_c}\mathbf{A^T} & \mathbf{Z}_m \\ \mathbf{D} & \mathbf{W}+\mathbf{Z}_u \end{bmatrix} \begin{bmatrix} \mathbf{I(t)} \\ \mathbf{M}(t) \end{bmatrix} = \begin{bmatrix} -\mathbf{V}_s - 2\mathbf{V}_p^i[\mathbf{1}]_{N_l} - 2\mathbf{V}_m^i[\mathbf{1}]_{3N_m} - 2\mathbf{A}\mathbf{V}_c^i[\mathbf{1}]_{N_n} - 2\mathbf{A}\mathbf{Z}_c\mathbf{I}_s \\ -\mathbf{G}\mathbf{I}_s(t) - 2\mathbf{V}_u^i \end{bmatrix}. \quad (10)$$

The hybrid TLM–PEEC 3-D solution consists of the vectors $\mathbf{I}(t)$ and $\mathbf{M}(t)$, representing N_l and $3N_m$ elements, respectively. The N_l and N_m values for the 3-D solution are numerically greater than those for the similar 2-D solution due to additional elements generated in the third dimension. The hybrid TLM–PEEC 2-D solution includes N_l and $2N_m$ elements, considering the planar vector components of magnetization. However, the standard PEEC solver includes an additional vector $\Phi(t)$ with a size of N_n, resulting in a computational benefit in the hybrid TLM–PEEC solver. The vector $\Phi(t)$ can be postprocessed at each time step using (8) if required. The initial values for the unknown incident voltage matrices $\mathbf{V}_p^i$, $\mathbf{V}_c^i$, and $\mathbf{V}_m^i$ should be set, and these matrices are then updated iteratively through linear TLM iterations using their corresponding reflective voltage matrices $\mathbf{V}_p^r$, $\mathbf{V}_c^r$, and $\mathbf{V}_m^r$ as described in Algorithm 1. Inside the algorithm, all sections and linear independent matrix process threads are executed in parallel to achieve maximum performance. According to transmission line theory, if the nonlinear relationship of a resistor is expressed as $V_u(t) = f_0(i_u(t))$, the voltage across the nonlinear element can be derived as follows [28]:

$$V_u^i(t+1) + V_u^r(t) = f_0\left(\frac{V_u^i(t+1) - V_u^r(t)}{Z_u}\right). \quad (11)$$

Equation (11) can be applied to the equivalent nonlinear magnetic circuit in Fig. 2(f) to obtain the following nonlinear equation, which can be used to update $\mathbf{V}_u^i(t+1)$ for the next

Algorithm 1: Parallel Hybrid TLM-PEEC Time-Domain Solver.

$\mathbf{V}_p^i, \mathbf{V}_c^i, \mathbf{V}_m^i, \mathbf{V}_u^i \leftarrow$ **Initialize incident matrices**.
$T_{max} \leftarrow$ **Set maximum time steps**.
for $t = 1 : T_{max}$
  $\mathbf{V}_s(t), \mathbf{I}_s(t) \leftarrow$ **Update source voltages and currents**.
  $\mathbf{I}(t), \mathbf{M}(t) \leftarrow$ **Solve** (10) **to update**.
  $\mathbf{I}_c(t) \leftarrow \mathbf{A}^T\mathbf{I}(t) + \mathbf{I}_s(t)$
  $\mathbf{I}_{c,sq}(t) \leftarrow$ **Diagonal matrix from** $\mathbf{I}_c(t)$
  $\mathbf{I}_{sq}(t) \leftarrow$ **Diagonal matrix from** $\mathbf{I}(t)$
  $\mathbf{M}_{sq}(t) \leftarrow$ **Diagonal matrix from** $\mathbf{M}(t)$

$$\text{Section I} \begin{cases} \mathbf{V}_p(t) \leftarrow 2\mathbf{V}_p^i(t) + \mathbf{Z}_p\mathbf{I}_{sq}(t) \\ \mathbf{V}_p^r(t) \leftarrow \mathbf{V}_p(t) - \mathbf{V}_p^i(t) \\ \mathbf{V}_p^i(t+1) \leftarrow -\mathbf{V}_p^r(t) \end{cases}$$

$$\text{Section II} \begin{cases} \mathbf{V}_c(t) \leftarrow 2\mathbf{V}_c^i(t) + \mathbf{Z}_c\mathbf{I}_{c,sq}(t) \\ \mathbf{V}_c^r(t) \leftarrow \mathbf{V}_c(t) - \mathbf{V}_c^i(t) \\ \mathbf{V}_c^i(t+1) \leftarrow \mathbf{V}_c^r(t) \end{cases}$$

$$\text{Section III} \begin{cases} \mathbf{V}_m(t) \leftarrow 2\mathbf{V}_m^i(t) + \mathbf{Z}_m\mathbf{M}_{sq}(t) \\ \mathbf{V}_m^r(t) \leftarrow \mathbf{V}_m(t) - \mathbf{V}_m^i(t) \\ \mathbf{V}_m^i(t+1) \leftarrow -\mathbf{V}_m^r(t) \end{cases}$$

$$\text{Section IV} \begin{cases} \mathbf{V}_u(t) \leftarrow 2\mathbf{V}_u^i(t) + \mathbf{Z}_u\mathbf{M}(t) \\ \mathbf{V}_u^r(t) \leftarrow \mathbf{V}_u(t) - \mathbf{V}_u^i(t) \\ \mathbf{V}_u^i(t+1) \leftarrow \textbf{Newton}-\textbf{Raphson} \\ (\mathbf{V}_u^i(t), \mathbf{V}_u^r(t)) \end{cases}$$

end

time step.

$$f(\mathbf{V}_u^i(t+1)) = \mathbf{V}_u^i(t+1) + \mathbf{V}_u^r(t) - \Omega(\mathbf{V}_u^i(t+1))\left(\frac{\mathbf{V}_u^i(t+1) - \mathbf{V}_u^r(t)}{\mathbf{Z}_u}\right) = 0. \tag{12}$$

This relationship presents a decoupled nonlinear equation, where each vector holds $3Nm$ elements representing the cartesian components of individual magnetic elements. This enables the separation between linear and nonlinear components of the hybrid TLM-PEEC model, leading to a parallel time-domain solution for nonlinear resistors, linear resistors, inductors, and capacitors in the equivalent circuit network. The nonlinear equation can be solved through an iterative method, and the N–R method is ideal, given the differentiability of the nonlinear equation and its quadratic convergence rate, which facilitates solving in fewer iterations. After differentiating (12) with respect to $\mathbf{V}_u^i(t+1)$, the Jacobian vector $J(\mathbf{V}_u^i(t+1))$ for the N–R implementation can be expressed as follows [30]:

$$J(\mathbf{V}_u^i(t+1)) = \frac{\partial f}{\partial \mathbf{V}_u^i(t+1)} = 1 - \frac{\Omega(|\mathbf{H}(t)|)}{\mathbf{Z}_u} - \frac{\partial \Omega}{\partial \mathbf{V}_u^i(t+1)}\left(\frac{\mathbf{V}_u^i(t+1) - \mathbf{V}_u^r(t)}{\mathbf{Z}_u}\right). \tag{13}$$

Algorithm 2: Decoupled N–R Solver.

Newton-Raphson $(\mathbf{V}_u^i(t), \mathbf{V}_u^r(t))$
$\Delta_x \leftarrow$ **Initialize step size**.
$\mathbf{V}_u^i(t+1) \leftarrow \mathbf{V}_u^i(t)$
$tolerance \leftarrow$ **Set convergence tolerance**.
$N_{max} \leftarrow$ **Set maximum iterations**.
for $k = 1 : N_{max}$
  $\mathbf{B}(t+1) \leftarrow$ **Calculate from** (15).
  $\mu_r(|\mathbf{H}(t+1)|) \leftarrow$ **Calculate from B-H relationship**.
  $\Omega(|\mathbf{H}(t+1)|) \leftarrow$ **Update from** (5).
  $f(\mathbf{V}_u^i(t+1)) \leftarrow$ **Update from** (12).
  $J(\mathbf{V}_u^i(t+1)) \leftarrow$ **Update from** (13) **and** (14).
  $\Delta_x \leftarrow -f(\mathbf{V}_u^i(t+1))/J(\mathbf{V}_u^i(t+1))$
  if $|\Delta_x| < tolerance$
    $\mathbf{V}_u^i(t+1) \leftarrow \mathbf{V}_u^i(t+1) + \Delta_x$
    break
  endif
  $\mathbf{V}_u^i(t+1) \leftarrow \mathbf{V}_u^i(t+1) + \Delta_x$
end

$$\frac{\partial \Omega}{\partial \mathbf{V}_u^i(t+1)} = \frac{\mu_0}{(\mu_r(|\mathbf{H}|) - 1)^2} \frac{\mathbf{B} - \mathbf{W} \cdot \left(\frac{\mathbf{V}_u^i(t+1) - \mathbf{V}_u^r(t)}{\mathbf{Z}_u^2}\right)}{\mathbf{B} - \mu_0\left(\frac{\mathbf{V}_u^i(t+1) - \mathbf{V}_u^r(t)}{\mathbf{Z}_u^2}\right)^2}. \tag{14}$$

The Jacobian calculation requires the determination of the magnetic flux density $\mathbf{B}(t)$, $\mu_r(|\mathbf{H}(t)|)$, and $\Omega(|\mathbf{H}(t)|)$ in terms of $\mathbf{V}_u^i(t+1)$. $\mathbf{B}(t)$ can be expressed using the unknown incident voltage vector and can be written as follows:

$$\mathbf{B}(t) = \mathbf{D}\mathbf{I}(t) + \mathbf{W}\left(\frac{\mathbf{V}_u^i(t+1) - \mathbf{V}_u^r(t)}{\mathbf{Z}_u}\right). \tag{15}$$

$\mathbf{H}(t)$ can be derived from $\mathbf{B}(t)$ through the B–H relationship of the magnetic material, and $\mu_r(|\mathbf{H}(t)|)$ can be determined using the relationship as follows:

$$\mathbf{B}(t) = \mu_0\mu_r(|\mathbf{H}(t)|)\mathbf{H}(t). \tag{16}$$

Equations (12)–(16) describe the relationships required to formulate N–R iterations, while $\Omega(|\mathbf{H}(t)|)$ can be calculated using (5). Algorithm 2 describes the decoupled N–R solver for the calculation of $\mathbf{V}_u^i$ for the next time step, and the relative tolerance, as well as the maximum iteration count $N_{\max}$ can be user-defined based on the required accuracy. The matrix architecture defined in this algorithm solves $3N_m$ matrix elements simultaneously, leading to the individual parallel solution of each nonlinear magnetic element. As illustrated in Algorithms 1 and 2, all the TLM iterations, including linear and nonlinear, can be updated in parallel, independently of each other. Since N_l and N_m are numerically larger values for 3-D systems, the PEEC linear system in (10) results in a larger dense matrix system. Therefore, it is challenging to achieve a computationally efficient solution. Reducing the order of the system is an efficient way to decrease computational time and resources while retaining the necessary accuracy.

This article has been accepted for inclusion in a future issue of this journal. Content is final as presented, with the exception of pagination.

IV. Reduced Order Modeling for the Proposed Hybrid TLM-PEEC Method

The order of the PEEC system provided in (10) can be reduced using the POD method [31] and this decoupled linear system can be expressed as $\mathbf{A}_0\mathbf{X}_0 = \mathbf{B}_0$, where $\mathbf{A}_0$ is the coefficient matrix, $\mathbf{B}_0$ is the constant vector, and $\mathbf{X}_0$ is the solution vector. Using data projection, $\mathbf{X}_0$ can be written as follows:

$$\mathbf{X}_0 = \Psi\mathbf{X}_r \tag{17}$$

where Ψ is the projection operator and $\mathbf{X}_r$ is the reduced-order solution vector with size *r*, where r $< N_l + 3N_m$. Ψ can be obtained using singular value decomposition (SVD) theory, and to start with it, a solution snapshot vector $\mathbf{X}_s$ needs to be formulated. Solution snapshots are obtained by solving the original system (10) for *N* time steps, and they can be arranged as follows to formulate $\mathbf{X}_s$:

$$\mathbf{X}_s = \left[\mathbf{X}^1, \mathbf{X}^2, \mathbf{X}^3 \ldots \mathbf{X}^N\right] \tag{18}$$

where $\mathbf{X}^N$ describes the Nth solution snapshot. SVD can be applied to $\mathbf{X}_s$, allowing it to be expressed using the decomposed matrices as follows:

$$\mathbf{X}_s = \mathbf{U}\Sigma\mathbf{V}^T = \sum_{i=1}^{N} \sigma_i \mathbf{u}_i \mathbf{v}_i^T \tag{19}$$

where Σ is the diagonal matrix with singular values ordered in descending order, each σ_i corresponds to the square root of the eigenvalues of the matrices $\mathbf{X}_s\mathbf{X}_s^T$ and $\mathbf{X}_s^T\mathbf{X}_s$. $\mathbf{U}$ and $\mathbf{V}$ are orthogonal matrices with $\mathbf{u}_i$ and $\mathbf{v}_i$ being the eigenvectors of $\mathbf{X}_s\mathbf{X}_s^T$ and $\mathbf{X}_s^T\mathbf{X}_s$. The columns of $\mathbf{U}$ correspond to the orthonormal basis for the solution space and the magnitude of each σ_i represents the degree of importance of the corresponding orthonormal column vector in spanning the solution space. Therefore, the first r columns of $\mathbf{U}$ contain the most important features of the system and a reduced-order model can be formulated using the below-defined projection operator

$$\Psi = \left[\mathbf{u}_1, \mathbf{u}_2, \mathbf{u}_3 \ldots \mathbf{u}_r\right]. \tag{20}$$

The lower-order system with size r can be defined using the projection operator as follows:

$$\mathbf{A}_r\mathbf{X}_r = \mathbf{B}_r \tag{21}$$

where $\mathbf{A}_r = \Psi^T\mathbf{A}_0\Psi$ and $\mathbf{B}_r = \Psi^T\mathbf{B}_0$. The reduced order can be solved with less computation effort, but it is challenging to map it to the corresponding nodes in the PEEC mesh due to the dimensionality difference. Therefore, it needs to be projected back to the higher order using (17) after the solution step to retain the same physical meaning at each point in the PEEC mesh. In Algorithm 1, instead of solving the full-order system in (10), the lower-order system in (21) can be solved to achieve higher performance.

V. Case Studies

In this section, two power system equipments are implemented to provide the accuracy and computational efficiency of the 3-D hybrid TLM–PEEC time-domain solver. The time-domain solver is implemented based on the matrix implementation and algorithms provided in Section II. The power system equipment geometries are discretized and implemented on GPU using CUDA to achieve maximum parallelism in the hybrid TLM-PEEC time domain solver.

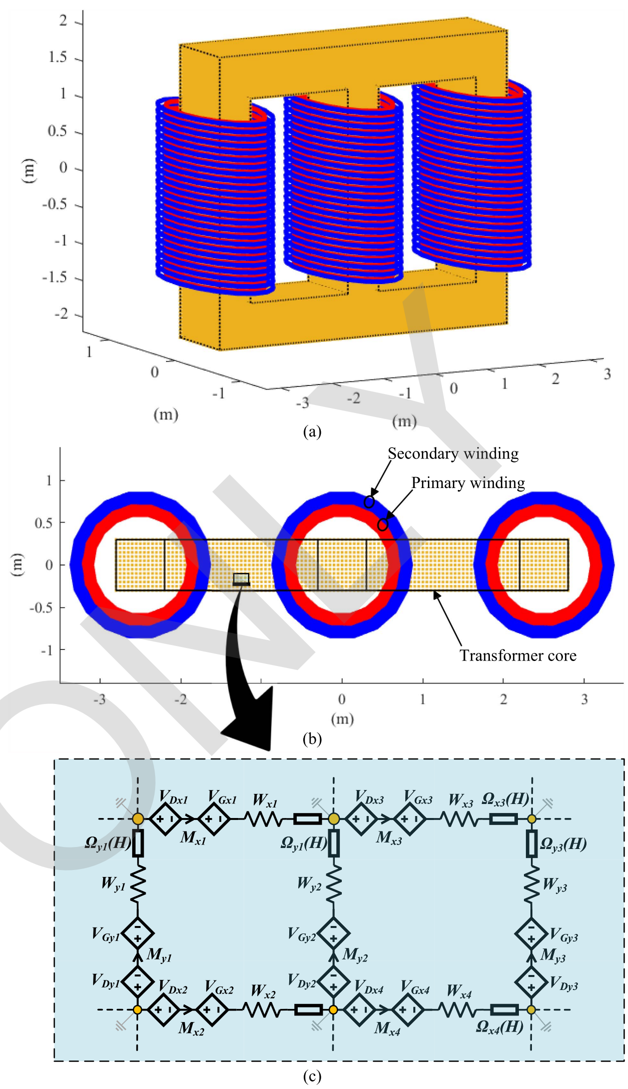

Fig. 3. 3-phase core-type 3-D transformer PEEC geometry: (a) side view, (b) top view, (c) PEEC equivalent circuit for the core; note that the PEEC nodes shown in (b) are fewer than the actual number of nodes utilized.

A. 3-Phase Core Type Transformer

A 3-phase core-type transformer was studied in this work with conductor-based multiturn coils as the primary and secondary winding for each phase, along with a solid ferromagnetic core, as illustrated in Fig. 3. Each winding is connected to a three-phase balanced circuit consisting of parasitic elements to perform the transient analysis of the hybrid TLM–PEEC transformer model as described in Fig. 4. Each primary winding is initially connected to a sinusoidal 60 Hz ac voltage source, and later in the simulation, second and fourth harmonics are injected to

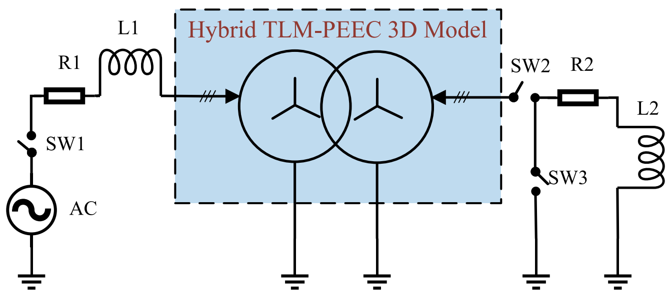

Fig. 4. 3-phase transformer external circuit.

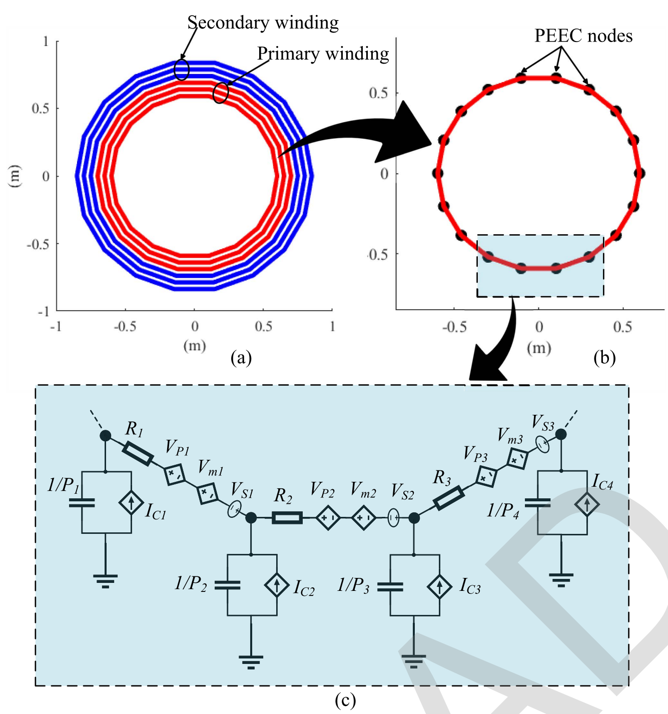

Fig. 5. 3-phase transformer winding geometry. (a) Top view for one phase. (b) Node mesh for a top layer turn. (c) PEEC equivalent circuit for a top layer turn.

enhance the analysis. Detailed simulation parameters, including external circuit and transformer details [40], are available in the appendix. Inside the hybrid TLM–PEEC model, the ferromagnetic core is modeled as a nonlinear magnetic material and rectangular volume cells are assigned to each magnetic element. Transformer windings are assumed as conductor wires, each discretized into segments, and the PEEC equivalent circuit is formulated as illustrated in Fig. 5.

An EMT case study is performed on the hybrid TLM–PEEC transformer model coupled to an external circuit, including open circuit, short circuit, and harmonic injections. The hybrid TLM–PEEC nonlinear solver is set to a relative tolerance of 10^{-5} to ensure reliable convergence, with a time step of 100 μs chosen for accuracy. The simulation runs for a total time of 250 ms, and within this period, the following events are triggered.

1) At $t = 0$ ms, $SW1$ is turned ON, and the transformer is energized through the primary windings while the secondary windings are open-circuited.
2) At $t = 60$ ms, $SW2$ is turned ON, and the transformer works with 3-phase balanced loads $R2$ and $L2$.
3) At $t = 110$ ms, the second and fourth harmonics are injected into the 3 phases of the voltage source V_{ac}.
4) At $t = 190$ ms, $SW3$ is turned on, and the secondary windings are short-circuited.

The case study was executed on a many-core GPU to achieve maximum parallelism and a multicore CPU to obtain relative CPU performance, as the benchmark Comsol simulation cannot be executed on a GPU. The Nvidia Tesla V100 GPU is used with CUDA to achieve maximum parallelism across the 5120 available cores. Partial element calculations were executed on the hardware using device functions implemented according to analytical formulas, while the matrix operations for addition and multiplication were implemented based on first principles. In addition, the cuSOLVER API was utilized to solve the linear system within the TLM iterations. The multicore CPU implementation was carried out on a PC featuring an Intel Xeon E5-2698 CPU boasting 40 cores, accompanied by 192 GB of RAM, and operating at a clock frequency of 2.2 GHz. Multicore CPU implementation was carried out using the pthread library, which allows the creation and management of concurrent processes in an efficient manner. The Comsol benchmark simulation was carried out on the same multicore CPU, with the software consistently aiming to utilize the maximum available CPU cores to achieve the highest performance, providing a parallel benchmark simulation to measure the performance of the proposed hybrid TLM-PEEC solver.

The simulation results from the hybrid TLM-PEEC GPU solver include electrical quantities from windings as well as field quantities from the magnetic core. Magnetic field results consist of the magnetic flux density (B) and the eddy current density of the core (J), with a comparison to the Comsol simulation illustrated in Fig. 6. All field quantities are extracted from $3N_m$ magnetic elements defined in the transformer core corresponding to Cartesian vector components. The eddy current density is calculated by postprocessing the electric field inside the core using analytical formulas provided in [41]. Meanwhile, the 3-phase voltages and currents from the transformer, describing the primary winding voltage (V_p), secondary winding voltage (V_s), primary winding current (I_p), and secondary winding current (I_s), are presented in Fig. 7, along with an accuracy comparison against Comsol. To further investigate the accuracy of the electrical parameters, Fast Fourier transform (FFT) results were obtained for the harmonic injection period, and these results are presented in Fig. 8. The errors in the figures represent the mean absolute percentage error (MAPE) between the proposed hybrid TLM-PEEC solver and the Comsol solver.

In the POD–TLM–PEEC method, reducing the order improves performance, but it decreases accuracy compared to the full-order model. The MAPE between the full-order and reduced-order models with different orders for Case 1 is illustrated in Fig. 9, along with the speedup for each order. The MAPE has decreased to less than 2% with an order of 16 or more. Therefore, the 16th-order model was chosen as the optimal model order to improve system performance while retaining accuracy.

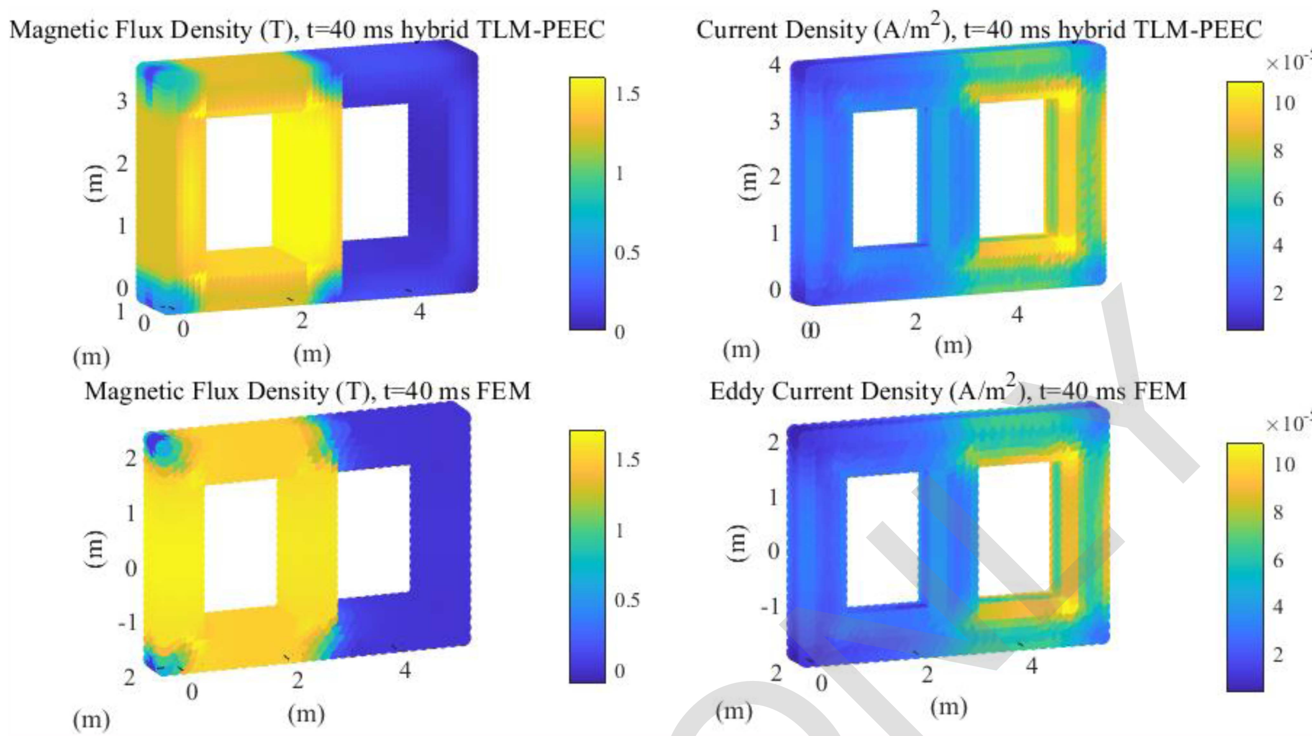

Fig. 6. Comparison of magnetic flux density and eddy current density between hybrid TLM-PEEC and Comsol models.

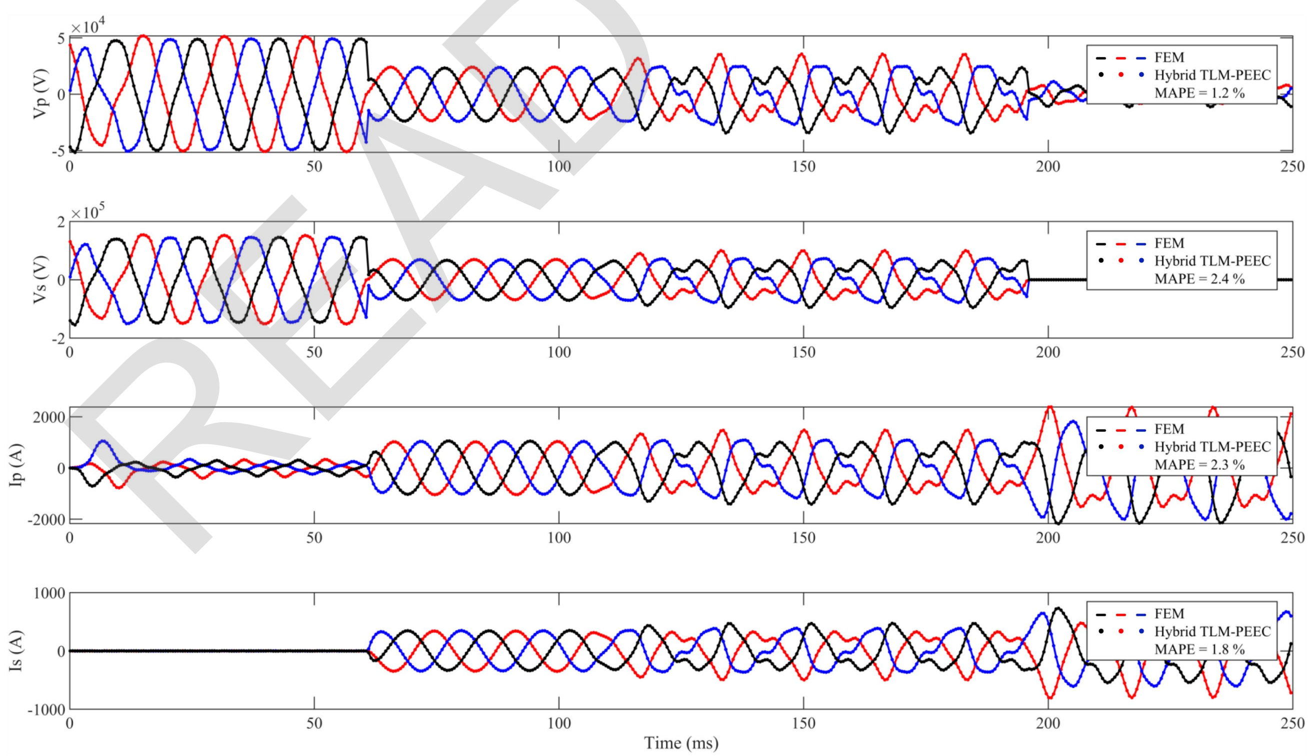

Fig. 7. Comparison of the proposed hybrid TLM-PEEC parallel numerical simulation and Comsol results for the 3-phase 3-D transformer model.

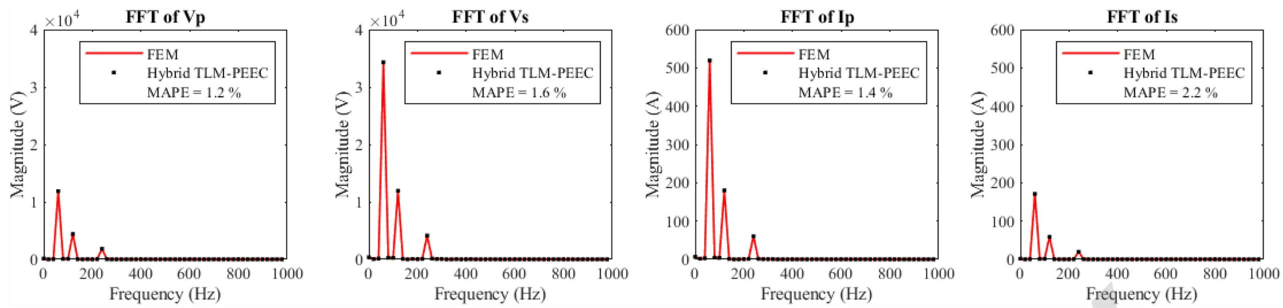

Fig. 8. Comparison of FFT results between the hybrid TLM-PEEC method and FEM during the harmonic injection period from 110 to 190 ms.

TABLE I
EXECUTION TIME AND SPEEDUP OF PROPOSED ARCHITECTURES ON MANY-CORE GPU AND MULTICORE CPU

Cases	Number of PEEC Nodes	Comsol™ Execution Time (s)	Hybrid TLM-PEEC on many-core GPU (full-order)		Hybrid TLM-PEEC on multi-core CPU (full-order)		POD-TLM-PEEC on many-core GPU (reduced-order)		POD-TLM-PEEC on multi-core CPU (reduced-order)	
			Execution Time (s)	Speedup¹	Execution Time (s)	Speedup²	Execution Time (s)	Speedup³	Execution Time (s)	Speedup⁴
1	7141	253.5	12.1	20.9	22.6	11.2	6.0	42.3	15.7	16.1
2	9562	308.2	14.9	20.6	28.2	10.9	7.7	40.0	19.7	15.6
3	12320	452.8	22.8	19.9	43.1	10.5	12.0	37.7	29.9	15.1
4	18242	1115.7	58.5	19.0	113.8	9.8	32.5	34.3	75.8	14.7
5	25961	1825.3	98.4	18.5	198.4	9.2	58.7	31.1	128.5	14.2

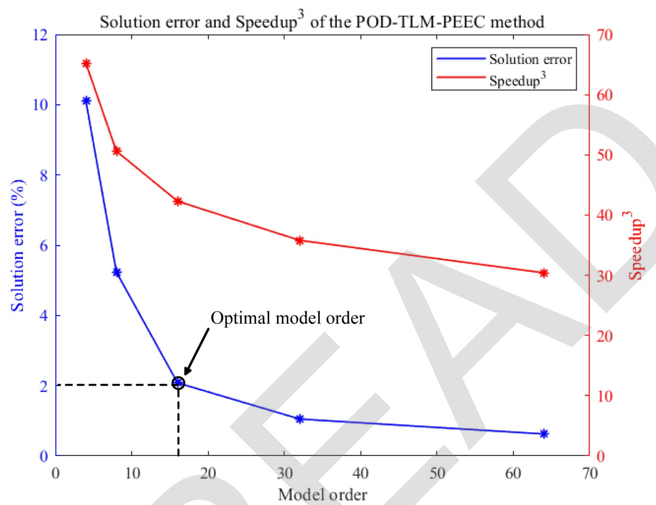

Fig. 9. Solution error and speedup^3 of the POD-TLM-PEEC method against the model order for Case 1.

Multiple simulations were conducted with varying mesh sizes to measure the performance of the proposed hybrid TLM–PEEC method and POD–TLM–PEEC method on the many-core GPU and multicore CPU, and these results were compared against benchmark COMSOL simulations. Different simulation cases and their corresponding elapsed times are recorded in Table I, showing speed-up improvements for GPU and CPU implementations on the parallel architectures. Speedup^1, Speedup^2, Speedup^3, and Speedup^4 demonstrate the elapsed time ratio of the hybrid TLM–PEEC GPU solver, hybrid TLM–PEEC CPU solver, POD–TLM–PEEC GPU solver, and POD–TLM–PEEC CPU solver against the COMSOL solver, respectively. The GPU solver demonstrates substantial speed-up improvements due to its large number of cores designed for parallel processing, combined with CUDA programming. Among the GPU implementations, the POD–TLM–PEEC solver achieved the highest performance as it provides greater computational benefits through the reduced order model.

B. High Voltage Insulator

A high-voltage insulator was studied using the proposed hybrid TLM–PEEC method as well as the POD–TLM–PEEC method to demonstrate their applicability for electrostatic applications. A high-voltage composite insulator rated at 110 kV is illustrated in Fig. 10(a), and a quasi-static simulation was conducted to analyze its static behavior over a given period of time. The composite insulator consists of a central rod made of fiber-reinforced plastic with a relative permittivity, $\epsilon_r = 5$ and an outer weather shed made of silicone rubber with a relative permittivity, $\epsilon_r = 3$. The metal fittings used for high-voltage energization are made of forged steel. The bottom metal fitting is connected to the ground, while the top metal fitting is connected to a sinusoidal 60 Hz ac voltage source, and later in the simulation, several harmonics are injected to enhance the simulation. Metal grading rings are installed around the sheds at both ends, and simulations were conducted with and without the grading rings to observe the electric field gradient along the insulator. The geometry was discretized using a fine-grained mesh, with each point in the mesh representing a PEEC node. As in the previous example, the same approach was followed to generate the PEEC equivalent circuit network, with small rectangular cells assigned to minimize the discretization error in the curved regions. Each adjacent PEEC node is connected through the PEEC equivalent circuit illustrated in Fig. 10(c), and partial element calculations

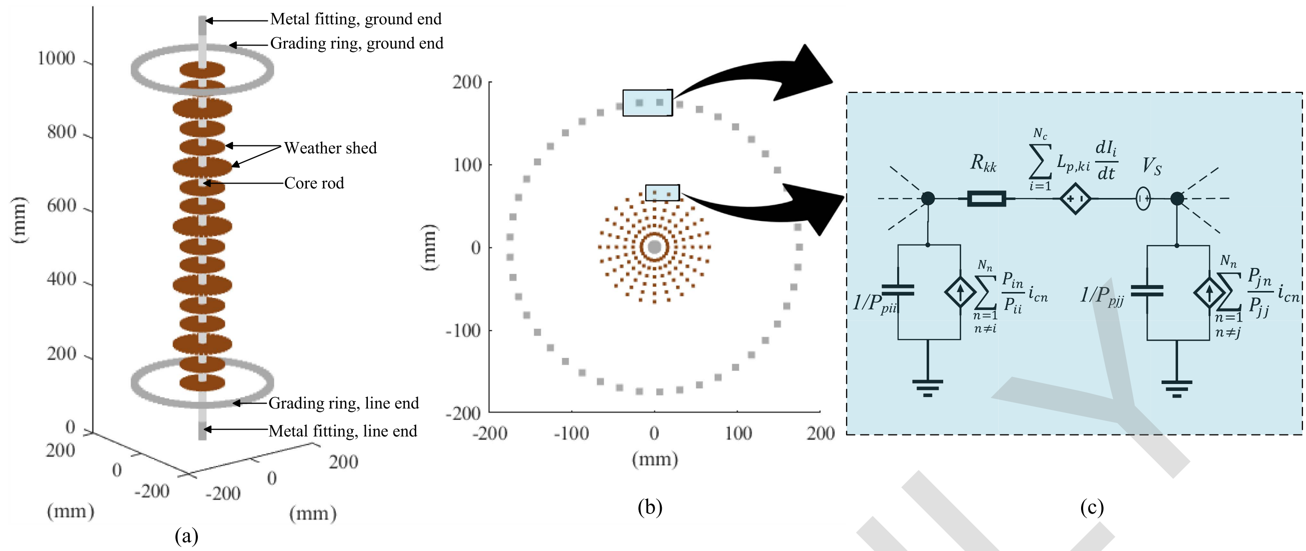

Fig. 10. High-voltage insulator PEEC geometry. (a) Side view. (b) Top view. (c) PEEC equivalent circuit between adjacent nodes; note that the PEEC nodes shown in (b) are fewer than the actual number of nodes utilized.

are adjusted based on material properties such as conductivity and relative permittivity. The central rod and weather sheds are discretized using small rectangular insulator elements as in Fig. 10(b), assuming they act as insulators with a conductivity of $\sigma = 1.0\times 10^{-14}$ S/m. Additional simulation details and geometry parameters are available in the appendix.

A quasi-static simulation was performed by applying a time-varying voltage between the metal fittings. The simulation runs for 100 ms, with the fundamental voltage applied to the top metal fitting at $t = 0$, and two harmonics injected at $t = 50$ ms, remaining until the end of the simulation. The case study was carried out on the many-core GPU using the hybrid TLM–PEEC method with a mesh consisting of 2249 nodes, utilizing a time step of 100 μs for the simulation. A similar benchmark case study was conducted using Comsol for accuracy comparison against the proposed hybrid TLM–PEEC method. The excitation electric potential over the simulation period and the electric potential distribution across the insulator at 55 ms are illustrated in Fig. 11, along with a comparison against Comsol. Electric potential distribution is derived using the nodal voltage at each point obtained from the hybrid TLM–PEEC GPU solver. The Comsol simulation took 8.1 s to solve the high voltage insulator, whereas the hybrid TLM–PEEC GPU solver accomplished the same in 0.8 s, resulting in a speedup of 10.1×. The POD–TLM–PEEC GPU solver achieved a 13.5× speedup, solving the case study in 0.6 s with the 16th-order model, while maintaining a 2% error between the full-order and reduced-order models. The performance was achieved through parallelism in the hybrid TLM–PEEC solver and the reduced-order benefits from the POD–TLM–PEEC solver, respectively.

The electric field inside the insulator is calculated using the analytical formulas presented in [41], and the electric field along the insulator rod is illustrated in Fig. 12, with a comparison against the electric field derived from Comsol. Calculating the electric field with and without grading rings reveals that, with

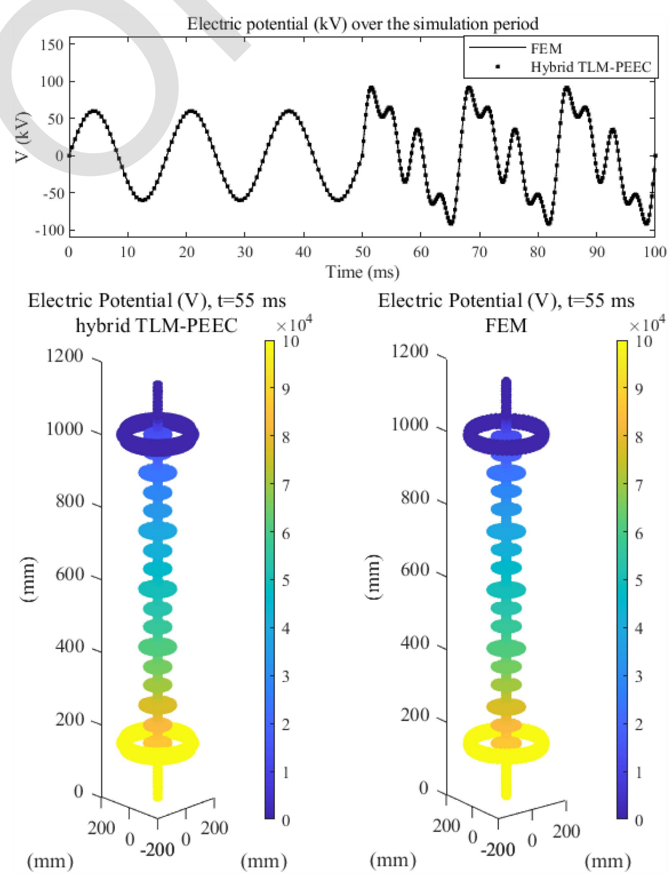

Fig. 11. Electric potential distribution of the high-voltage insulator.

the grading rings, the electric field is smoothed over the insulator rod. Meanwhile, without grading rings, it is concentrated at the ends of the insulator, leading to flashover. Electric field norm calculations show a relative error of 2.1% compared to

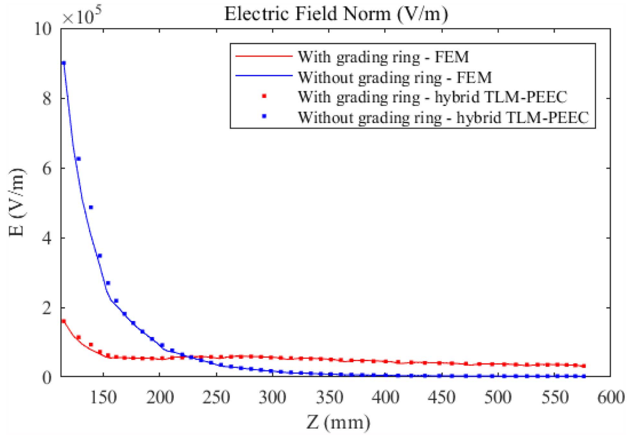

Fig. 12. Electric field norm along the central axis of the insulator.

Comsol, demonstrating the validity of the proposed TLM–PEEC approach over static applications.

VI. Conclusion

In this article, a parallel hybrid TLM–PEEC 3-D solver has been proposed for EMT analysis of nonlinear magnetic systems. As the 3-D solver encounters higher computational burden, a MOR technique is proposed for the hybrid TLM–PEEC 3-D solver to achieve greater performance benefits. The hybrid TLM–PEEC parallel solver is implemented by solving parasitic elements in the standard PEEC equivalent circuit using the respective TLM models, leading to a reduction in the size of the coefficient matrix of the linear matrix equation system from $N_l + N_n + 3N_m$ to $N_l + 3N_m$. The nonlinear elements in the system, representing $3N_m$ nonlinear magnetic elements, are decoupled from the linear network using TLM, and the nonlinear matrix equation is then solved independently using N–R iterations. The parallel hybrid TLM–PEEC time domain solver and decoupled N–R solver algorithms are presented in this work for 3-D EM systems, along with their detailed implementations. The POD–TLM–PEEC method has been proposed to enhance system performance by solving a reduced-order model without compromising accuracy. The proposed methods have been applied to study EMTs in a 3-phase core-type transformer coupled to an external circuit and to conduct quasi-static simulations on a high-voltage insulator. Transformer geometry details, including the winding structure and its equivalent PEEC models, are described, and the results from EMT simulations are presented, along with accuracy and performance comparisons against Comsol. The numerical results demonstrate accuracy with a MAPE of less than 2% over the simulation period, achieving a maximum speedup of 42.3× on the many-core GPU and 16.1× on the multicore CPU with the reduced-order model, while the full-order model achieved speedups of 20.9× and 11.2×, respectively. The high voltage insulator geometry and numerical results are presented, achieving similar outcomes to Comsol while attaining a speedup of 13.5× with the reduced-order model and 10.1× with the full-order model. The hybrid TLM–PEEC approach is applicable for both static and dynamic EM applications, and its decoupled parallel implementation enhances model solution performance while maintaining the required accuracy. The POD–TLM–PEEC approach removes unnecessary features of the system, leading to a reduced-order problem, and has demonstrated better performance on parallel computing hardware, making it suitable for real-time hardware simulations of power system apparatus.

Appendix
Case Study Parameters

Transformer parameters: The yoke length is 5.6 m, the limb length is 4.0 m, and the cross-sectional area of each winding is 0.0001 m ^{2}. In each phase, the primary winding consists of 600 turns and the secondary winding consists of 200 turns. V_{AC} = 53.033sin(120π t) kV, R_1 = 25 Ω, R_2 = 200 Ω, and $L_1 = L_2$ = 36 mH. The magnitude of the injected second and fourth harmonics are 21.76 and 10.88 kV at frequencies of 120 and 240 Hz, respectively.

HV Insulator parameters: The core rod length is 1.15 m, and the diameters of the alternating weather sheds are 0.096 and 0.136, respectively. Between the metal fittings, V_{AC} = 60sin(120πt) kV is applied, and the magnitudes of the injected second and fourth harmonics are 40 and 30 kV at frequencies of 120 and 240 Hz, respectively.

References

[1] *IEEE Guide for Power System Protection Testing*, IEEE Standard C37.233-2023 (Revision of IEEE Standard C37.233-2009), Sep. 2023, pp. 1–135.
[2] Z. Mazloom, N. Theethayi, and R. Thottappillil, "A method for interfacing lumped-circuit models and transmission-line system models with application to railways," *IEEE Trans. Electromagn. Compat.*, vol. 51, no. 3, pp. 833–841, Aug. 2009.
[3] J. Faiz, B. Abed-Ashtiani, and M. Byat, "Lumped complete equivalent circuit of a coreless high-frequency transformer," *IEEE Trans. Magn.*, vol. 33, no. 1, pp. 703–707, Jan. 1997.
[4] M. Brignone, F. Delfino, R. Procopio, M. Rossi, and F. Rachidi, "Evaluation of power system lightning performance, Part I: Model and numerical solution using the PSCAD-EMTDC platform," *IEEE Trans. Electromagn. Compat.*, vol. 59, no. 1, pp. 137–145, Feb. 2017.
[5] S. Südekum and M. Leone, "Rigorous modal circuit synthesis including modal coupling for linear, time-invariant, and passive electromagnetic systems," *IEEE Trans. Electromagn. Compat.*, vol. 62, no. 5, pp. 2024–2035, Oct. 2020.
[6] H. D. Bruns, C. Schuster, and H. Singer, "Numerical electromagnetic field analysis for EMC problems," *IEEE Trans. Electromagn. Compat.*, vol. 49, no. 2, pp. 253–262, May 2007.
[7] A. E. Ruehli, "Inductance calculations in a complex integrated circuit environment," *IBM J. Res. Develop.*, vol. 16, no. 5, pp. 470–481, Sep. 1972.
[8] A. Ruehli and P. Brennan, "Efficient capacitance calculations for three-dimensional multiconductor systems," *IEEE Trans. Microw. Theory Techn.*, vol. MTT-21, no. 2, pp. 76–82, Feb. 1973.
[9] A. E. Ruehli, "Equivalent circuit models for three-dimensional multiconductor systems," *IEEE Trans. Microw. Theory Techn.*, vol. MTT-22, no. 3, pp. 216–221, Mar. 1974.
[10] A. Ruehli and H. Heeb, "Circuit models for three-dimensional geometries including dielectrics," *IEEE Trans. Microw. Theory Techn.*, vol. 40, no. 7, pp. 1507–1516, Jul. 1992.
[11] G. Antonini, M. Sabatini, and G. Miscione, "PEEC modeling of linear magnetic materials," in *Proc. IEEE Int. Symp. Electromagn. Compat.*, Portland, OR, USA, Aug. 2006, pp. 93–98.
[12] D. Romano and G. Antonini, "Quasi-static partial element equivalent circuit models of linear magnetic materials," *IEEE Trans. Magn.*, vol. 51, no. 7, Jul. 2015, Art. no. 7002115.

[13] A. Musing, J. Ekman, and J. W. Kolar, "Efficient calculation of non-orthogonal partial elements for the PEEC method," *IEEE Trans. Magn.*, vol. 45, no. 3, pp. 1140–1143, Mar. 2009.

[14] D. Romano and G. Antonini, "Augmented quasi-static partial element equivalent circuit models for transient analysis of lossy and dispersive magnetic materials," *IEEE Trans. Magn.*, vol. 52, no. 5, May 2016, Art. no. 7003911.

[15] L. Lombardi, P. Belforte, and G. Antonini, "Digital wave simulation of quasi-static partial element equivalent circuit method," *IEEE Trans. Electromagn. Compat.*, vol. 59, no. 2, pp. 429–438, Apr. 2017.

[16] D. Romano, G. Antonini, and A. E. Ruehli, "Time-domain partial element equivalent circuit solver including non-linear magnetic materials," *IEEE Trans. Magn.*, vol. 52, no. 9, Sep. 2016, Art. no. 7004911.

[17] L. Lombardi, D. Romano, and G. Antonini, "Analytical formula for the magnetic-to-electric field coupling of magnetization in the partial element equivalent circuit method," *IEEE Trans. Magn.*, vol. 54, no. 10, Oct. 2018, Art. no. 2500712.

[18] D. Romano, I. Kovačević-Badstübner, M. Parise, U. Grossner, J. Ekman, and G. Antonini, "Rigorous DC solution of partial element equivalent circuit models including conductive, dielectric, and magnetic materials," *IEEE Trans. Electromagn. Compat.*, vol. 62, no. 3, pp. 870–879, Jun. 2020.

[19] R. Torchio, M. Nolte, S. Schöps, and A. E. Ruehli, "A spline-based partial element equivalent circuit method for electrostatics," *IEEE Trans. Dielectrics Elect. Insul.*, vol. 30, no. 2, pp. 594–601, Apr. 2023.

[20] D. Daroui and J. Ekman, "PEEC-based simulations using iterative method and regularization technique for power electronic applications," *IEEE Trans. Electromagn. Compat.*, vol. 56, no. 6, pp. 1448–1456, Dec. 2014.

[21] G. Andrieu, A. Reineix, and J. Panh, "A numerical methodology for the prediction of the near-field parasitic electromagnetic emissions of solar panels," *IEEE Trans. Electromagn. Compat.*, vol. 51, no. 4, pp. 919–927, Nov. 2009.

[22] A. Ruehli, "Partial element equivalent circuit (PEEC) method and its application in the frequency and time domain," in *Proc. Symp. Electromagn. Compat.*, Santa Clara, CA, USA, 1996, pp. 128–133.

[23] S. Safavi and J. Ekman, "A hybrid PEEC-SPICE method for time-domain simulation of mixed nonlinear circuits and electromagnetic problems," *IEEE Trans. Electromagn. Compat.*, vol. 56, no. 4, pp. 912–922, Aug. 2014.

[24] J. Cao et al., "Lightning surge analysis of transmission line towers with a hybrid FDTD-PEEC method," *IEEE Trans. Power Del.*, vol. 37, no. 2, pp. 1275–1284, Apr. 2022.

[25] P. B. Johns and R. L. Beurle, "Numerical solution of 2-dimensional scattering problems using a transmission-line matrix," *Proc. Inst. Elect. Eng.*, vol. 118, no. 9, pp. 1203–1208, Sep. 1971.

[26] P. B. Johns and M. O'Brien, "Use of the transmission-line modelling (T.L.M.) method to solve non-linear lumped networks," *Radio Electron. Eng.*, vol. 50, no. 1/2, pp. 59–70, Jan. 1980.

[27] S. Y. R. Hui and C. Christopoulos, "Numerical simulation of power circuits using transmission-line modelling," *Proc. Inst. Elect. Eng., Phys. Sci., Meas. Instrum., Manage. Educ.*, vol. 137, no. 6, pp. 379–384, Nov. 1990.

[28] V. Dinavahi, "Transient analysis of systems with multiple nonlinear elements using TLM," *IEEE Trans. Power Syst.*, vol. 19, no. 4, pp. 2102–2103, Nov. 2004.

[29] P. Liu and V. Dinavahi, "Real-time finite-element simulation of electromagnetic transients of transformer on FPGA," *IEEE Trans. Power Del.*, vol. 33, no. 4, pp. 1991–2001, Aug. 2018.

[30] M. Ranasinghe and V. Dinavahi, "Partial element equivalent circuit based parallel electromagnetic transient simulation on GPU," *IEEE Trans. Magn.*, vol. 60, no. 10, Oct. 2024, Art. no. 7001509.

[31] J. L. Lumley, "The structure of inhomogeneous turbulent flows," in *Proc. Atmos. Turbulence Radio Wave Propag.*, Nauka, Moscow, 1967, pp. 166–178.

[32] S. Banerjee, J. Cole, and K. Jensen, "Nonlinear model reduction strategies for rapid thermal processing systems," *IEEE Trans. Semicond. Manuf.*, vol. 11, no. 2, pp. 266–275, May 1998.

[33] M. N. Albunni, V. Rischmuller, T. Fritzsche, and B. Lohmann, "Model-order reduction of moving nonlinear electromagnetic devices," *IEEE Trans. Magn.*, vol. 44, no. 7, pp. 1822–1829, Jul. 2008.

[34] S. Clénet, T. Henneron, and N. Ida, "Reduction of a finite-element parametric model using adaptive POD methods — Application to uncertainty quantification," *IEEE Trans. Magn.*, vol. 52, no. 3, Mar. 2016, Art. no. 7000704.

[35] J. Guo, P. Liu, V. Dinavahi, and W. Yang, "Model order reduction for real-time FPGA-based finite element transient simulation of three-phase transformer," *IEEE Open Access J. Power Energy*, vol. 9, pp. 328–339, 2022.

[36] V. Dinavahi and N. Lin, *Parallel Dynamic and Transient Simulation of Large-Scale Power Systems*. Switzerland AG: Springer Nature, 2022, pp. 1–492.

[37] R.-B. Wu, C.-N. Kuo, and K. K. Chang, "Inductance and resistance computations for three-dimensional multiconductor interconnection structures," *IEEE Trans. Microw. Theory Techn.*, vol. 40, no. 2, pp. 263–271, Feb. 1992.

[38] G. Zhong and C.-K. Koh, "Exact closed-form formula for partial mutual inductances of rectangular conductors," *IEEE Trans. Circuits Syst. I, Fundam. Theory Appl.*, vol. 50, no. 10, pp. 1349–1352, Oct. 2003.

[39] A. Ruehli, G. Antonini, and L. Jiang, "Computation of partial coefficients of potential," in *Circuit Oriented Electromagnetic Modeling Using the PEEC Techniques*. Hoboken, NJ, USA: Wiley, 2017, pp. 409–421.

[40] Joint Working Group A2/C4.39, "Electrical transient interaction between transformers and the power system Part 1 – expertise," International Council on Large Electric Systems (CIGRE), Tech. Rep. 577A, Apr. 2014.

[41] D. Romano, G. Antonini, L. Lombardi, U. Grossner, and I. Kovačević-Badstübner, "Analytical formulas for the computation of the electric field in the partial element equivalent circuit method with conductive, dielectric, and magnetic media," *IEEE Trans. Magn.*, vol. 55, no. 10, Oct. 2019, Art. no. 7000913.

Madhawa Ranasinghe (Student Member, IEEE) received the B.Sc. degree (Hons.) in electronic and telecommunication engineering from the University of Moratuwa, Colombo, Sri Lanka, in 2019. He is currently working toward the M.Sc. degree in electrical and computer engineering with the University of Alberta, AB, Canada.

His research interests include computational electromagnetics, high-performance simulations, and parallel and distributed computing.

Venkata Dinavahi (Fellow, IEEE) received the B.Eng. degree in electrical engineering from Visvesvaraya National Institute of Technology (VNIT), Nagpur, India, the M.Tech. degree in electrical engineering from the Indian Institute of Technology (IIT) Kanpur, India, and the Ph.D. degree in electrical and computer engineering from the University of Toronto, ON, Canada.

He is currently a Professor with the Department of Electrical and Computer Engineering, University of Alberta, Edmonton, AB, Canada. His research interests include real-time simulation of power systems and power electronic systems, electromagnetic transients, device-level modeling, artificial intelligence machine learning, large-scale systems, and parallel and distributed computing.

Prof. Dinavahi is a Fellow of the Engineering Institute of Canada (EIC) and the Asia-Pacific Artificial Intelligence Association (AAIA). He is a Professional Engineer (P.Eng.) in the province of Alberta, Canada.